Carbon and oxygen isotope records from the southern Eurasian Seaway following the Triassic-Jurassic boundary: Parallel long-term enhanced carbon burial and seawater warming

Stephen P. Hesselbo, Christoph Korte, Clemens V. Ullmann, Anders L. Ebbesen

PII: S0012-8252(19)30659-2

DOI: https://doi.org/10.1016/j.earscirev.2020.103131

Reference: EARTH 103131

To appear in: *Earth-Science Reviews*

Received date: 4 October 2019

Revised date: 6 February 2020

Accepted date: 13 February 2020

Please cite this article as: S.P. Hesselbo, C. Korte, C.V. Ullmann, et al., Carbon and oxygen isotope records from the southern Eurasian Seaway following the Triassic-Jurassic boundary: Parallel long-term enhanced carbon burial and seawater warming, *Earth-Science Reviews*(2020), https://doi.org/10.1016/j.earscirev.2020.103131

Carbon and oxygen isotope records from the southern Eurasian Seaway following the Triassic-Jurassic boundary: parallel long-term enhanced carbon burial and seawater warming

Stephen P. Hesselbo[a,*], Christoph Korte[b], Clemens V. Ullmann[a,b], Anders L. Ebbesen[b],

[a] Camborne School of Mines and Environment and Sustainability Institute, University of Exeter, Penryn Campus, Treliever Road, Penryn, Cornwall, TR10 9FE, UK

[b] Department of Geosciences and Natural Resource Management, University of Copenhagen, Øster Voldgade 10, 1350 Copenhagen-K, Denmark

*email: s.p.hesselbo@exeter.ac.uk

Keywords

Hettangian, Sinemurian, hydrothermal alteration, calcite fossils, UK, CAMP

ABSTRACT

Fossil shells of benthos and nektobenthos have been shown to be faithful recorders of seawater carbon- and oxygen-isotope geochemistry, and thus also useful to track the relationship between carbon cycle and palaeotemperature. In this study we present an extensive dataset from Lower Jurassic (Hettangian and lower Sinemurian) mollusc and brachiopod hard parts collected from biostratigraphically well-calibrated UK coastal outcrops (Bristol Channel and Hebrides basins). These basins lay palaeogeographically in the southern part of the Laurasian Seaway that connected the Tethys and Boreal oceans. All samples have been subject to screening for diagenesis on the basis of elemental composition, light microscopy, and SEM observations. In the case of some localities within the Hebrides Basin, alteration by hydrothermal systems around Paleogene intrusions has led to re-setting of carbonate oxygen isotopes, but the original carbon isotope values from the shells are largely preserved. Above the prominent and apparently short-lived, ~3 per mil $\delta^{13}C_{carb}$ amplitude positive carbon-isotope excursion (CIE) that occurs immediately above the Triassic-Jurasic (T-J) boundary (in the *tilmanni* ammonite biozone), a pronounced negative CIE (the so-called Main Negative CIE) spans the entire Hettangian Stage. At the Hettangian-Sinemurian boundary, and through the lower Sinemurian, the carbon-isotope values of the skeletal carbonate again trend towards progressively more positive values, but representing a time of several million years. The heaviest $\delta^{13}C_{carb}$ values of about ~ +4.3 per mil are evident towards the top of the lower Sinemurian and are comparable with values observed from the *tilmanni* Zone, and from the lower Toarcian, higher in the Jurassic. This long-term positive hump, which confirms trends derived from bulk organic matter carbon-isotope records, is supporting evidence of prolonged enhanced organic carbon burial that is inferred to have occurred in the extensive system of lacustrine and marine rifts that traversed a fragmenting Pangaea after emplacement of the Central Atlantic Magmatic Province. In parallel, oxygen-isotope values of the skeletal carbonate show a continuous downward trend from the lower part of the Hettangian (~ -1 per mil $\delta^{18}O_{carb}$ in the *planorbis* Zone) to the top of the lower Sinemurian (~ –4 per mil $\delta^{18}O_{carb}$ in the higher *turneri* Zone). Oxygen-isotope values may be interpreted as due to gradually increasing palaeotemperature, and/or addition of a meteoric or cryospheric water component; in the case of the Laurasian Seaway, palaeoceanographic and palaeoecological considerations point towards a dominant palaeotemperature signal. Consequently, any atmospheric carbon-dioxide drawdown effect on global palaeotemperatures, as suggested by progressively increasing $\delta^{13}C_{carb}$ values, and assuming a

constant silicate weathering sink, was more than counterbalanced in the seaway by regional processes that led to significantly warmer bottom water temperatures.

1. Introduction

In the wake of the Late Triassic mass extinction, which was likely driven by large-scale flood basalt volcanism, the Hettangian carbon cycle was subject to significant perturbation on both short and long timescales (e.g., McHone, 1996; Marzoli et al., 1999; Pálfy et al., 2001; Hesselbo et al., 2002; Ruhl et al., 2009; Bartolini et al., 2012; Al-Suwaidi et al., 2016; Korte et al., 2019). Most of our knowledge of the Hettangian carbon-cycle changes is derived from bulk marine organic matter records of carbon isotopes (van de Schootbrugge et al., 2009; Ruhl et al., 2010; Bartolini et al., 2012), with some bulk marine carbonate data also available (Bachan et al., 2012; Clemence et al., 2010, Yager et al., 2017). The succeeding marine carbon-isotope characteristics of the transition from the Hettangian into the Sinemurian are, in contrast, more sparsely and incompletely documented (e.g. Jenkyns et al., 2002; Porter et al., 2014; Jenkyns and Weedon, 2013; Hüsing et al., 2014; Xu et al., 2016; van de Schootbrugge et al., 2019, Schöllhorn et al., 2020; Storm et al., 2020).

Shells of low-Mg calcite (LMC) macrofossils have also been used as archives of marine carbon-isotope and oxygen-isotope trends and excursions, albeit at significantly lower resolution than for bulk records (e.g. van de Schootbrugge et al., 2007; Korte et al., 2009; Korte and Hesselbo, 2011). The present paper extends previous work on LMC macrofossils from the lower part of the Hettangian, and presents a greatly expanded dataset based upon samples from that point and through the lower Sinemurian successions from several basins around the UK (in Somerset, S Wales, Morvern and the Hebrides). Because many of the samples in the Hebrides come from locations affected by the Paleogene North Atlantic Large Igneous Province, we also examine the effects of thermal metamorphism and hydrothermal systems on macrofossil isotopic and elemental values.

2. Localities, stratigraphy, and depositional settings

The locations sampled for calcite fossils are (Fig. 1): St Audrie's Bay to East Quantoxhead (Somerset, England); Nash Point (Glamorgan, S Wales); Ardnish and Boreraig (Isle of Skye, Scotland); Hallaig Waterfall (Isle of Raasay, Scotland), and; Lochaline

(Morvern, Scotland). Full map grid references together with latitudes and longitudes for the sampled locations are provided below (sections 2.1–2.5). All successions are biostratigraphically well-studied (see Page, 1992, 1994, 2005, 2010; Hesselbo et al., 1998; Bloos and Page, 2002; Figs. 2 and 3, and associated dataset). Palaeogeographically, all sampled locations sit within the N-S oriented Laurasian Seaway that connected the equatorial Tethys Ocean with the Boreal Ocean and during the earliest Jurassic these locations had a palaeolatitude of ~ 40°N (Fig. 1; Bjerrum et al., 2001). The English and Welsh sections studied here lie within the Bristol Channel Basin, an E-W oriented Mesozoic extensional basin, whilst the Scottish localities are all within the Hebrides Basin, a Triassic-Jurassic extensional basin, with a predominant N-S orientation — see Ziegler (1990), Coward et al. (2003) and Stoker et al. (2016) for overview.

2.1. Somerset, England

The coastal exposures at St Audrie's Bay and East Quantoxhead (UK grid reference ST 102434 to 136442; 1″ N 003° 17′ 10.23″ W to 51°11'26.94"N 3°14'13.12"W; Figs. 1 and 2) have long been of interest for their record of the Triassic-Jurassic boundary, the overlying Hettangian strata, and the Hettangian-Sinemurian boundary. As a result, this section is biostratigraphically, magnetostratigraphically, chemostratigraphically, and cyclostratigraphically very well investigated (Palmer, 1972; Whittaker and Green, 1984; Warrington and Ivimey-Cook 1995; Hesselbo et al., 2002, 2004; Page, 2005, 2010; Deenen et al., 2010; Ruhl et al., 2010; Hüsing et al., 2014; Xu et al., 2016; Weedon et al., 2018, 2019). The whole succession is marine hemipelagic and comprises rhythmically bedded limestone, marl, and shale. The section at East Quantoxhead provides the Global Stratotype Section and Point (GSSP) for the base of the Sinemurian Stage (Bloos and Page, 2002); for the present study sampling was focussed on the middle part of the Hettangian and Hettangian-Sinemurian boundary interval.

2.2. Glamorgan, Wales

The rhythmically bedded limestone, marl, and laminated shale succession of Hettangian and Sinemurian age at Nash Point is located on the Monknash Coast at Vale of Glamorgan in South Wales (SS 914 682, 51°24'12.54"N 3°33'44.56"W; Fig. 1). The lithostratigraphy and biostratigraphy at this location is based on Trueman (1920, 1922, 1930),

Hodges (1986), Wilson et al. (1990) and Sheppard (2006). The succession, particularly the *bucklandi* Zone, is rich in thick-shelled ostreoid bivalves of the genus *Gryphaea*. Many of the specimens are silicified at this location, but unaltered shell calcite is also present.

2.3. Morvern, Scotland

The Hettangian to Sinemurian age succession at Lochaline, Morvern, Scotland (Hesselbo et al., 1998), is mainly exposed in three stream sections (Allt na Samhnachain [NM 69443 46024, 56°32'56.71"N 5°45'12.63"W], Allt Leacach [NM 69374 45329, 56° 32′ 35.44″ N 005° 45′ 11.37″ W], and Allt Mor [NM 69252 43383, 56° 31′ 33.48″ N 005° 44′ 37.24″ W]; Figs. 1 and 3). This succession comprises a top-Hettangian to lower Sinemurian rhythmically bedded limestone-marl succession of hemipelagic origin in the lower part, with the upper part (top lower Sinemurian *turneri* Zone) comprising thickly bedded shallow-marine mudstone-sandstone facies (Fig. 3). The *semicostatum* Zone is strongly condensed here. *Gryphaea* is very abundant in the lowest Sinemurian (*bucklandi* Zone). The Hettangian-Sinemurian boundary in Allt Leacach lies between bed 17 (highest occurrence of *Schlotheimia similis*) and bed 37, the lowest occurrence of *Vermiceras conybeari,* and its position corresponds approximately to the lowest occurrence of *Gryphaea* (Hesselbo et al., 1998).

2.4. Boreraig and Ardnish, Isle of Skye, Scotland

Two localities were sampled on the Isle of Skye (Fig. 1). At Boreraig (NG 62116 16237, 57°10'30.47"N 5°56'17.48"W) the succession comprises rhythmically bedded, shallow marine shale, mudstone and sandstone of Hettangian and Sinemurian age in which the *lyra* Subzone of the *semicostatum* Zone is stratigraphically expanded and contains abundant *Gryphaea* (Hallam, 1959; Hesselbo et al., 1998; Hesselbo and Coe, 2000). The succession at Ardnish (NG 68156 24562, 57° 15′ 10.03″ N 005° 50′ 43.12″ W) is of Sinemurian age (*semicostatum* Zone) and comprises mudstone and sandstone and a distinctive bed of oolitic ironstone (the Ardnish Ironstone; Hallam, 1959). *Gryphaea* is the common bivalve through this interval. In the higher beds, silicification of the macrofossils has occurred (Morton and Hudson, 1995; Hesselbo et al., 1998). Both localities are in moderate proximity to the outcrop of the Paleogene-age Beinn an Dubhaich granite pluton, ~ 2.6 km to the SSE in the case of

Boreraig and ~ 7.0 km to the WNW in the case of Ardnish (Hoersch, 1981; Holness, 1997; Holness and Fallick, 1997; Fig. 1).

2.5. Hallaig Waterfall, Isle of Raasay, Scotland

The section at Hallaig Waterfall, Raasay (NG59420 38680, 57° 22′ 29.23″ N 006° 00′ 12.59″ W), comprises a lower Sinemurian succession of shallow marine mudstone and sandstone assigned to the *semicostatum* and *turneri* zones (Figs. 1 and 3; Hallam, 1959; Morton and Hudson, 1995; Hesselbo et al., 1998). *Gryphaea* occurs abundantly here through the *semicostatum* Zone (Fig. 3) and allows an unusually high-resolution record to be constructed. Brachiopods are also common and belemnites occur.

3. Materials and methods

Fossils with low-Mg calcite (LMC) shells were collected in the field, including mainly ostreoids, with some *Plagiostoma*, pectinids, belemnites, and brachiopods. Results reported here are from specimens prepared and analysed at the Department of Geosciences and Natural Resource Management of the University of Copenhagen (see associated dataset).

Shells composed of low-Mg calcite are relatively resistant to diagenesis and can carry palaeoenvironmental information. Following well established protocols developed by many authors, as summarized in Ullmann and Korte (2015), samples were carefully screened to evaluate potential post-depositional alteration. In the present study, preparation of shell materials follows the method documented in Korte et al. (2009), and is described here only briefly. Splinters of bivalve shells were taken using a needle. The aliquots were inspected under a binocular microscope and using SEM (see Samtleben et al., 2001; Cochran et al., 2010). Only those shells with smooth-textured surfaces were regarded well preserved (e.g. Fig. 4 A–D). Freshly fractured inner fragments from belemnites were inspected using a binocular microscope and SEM. Only those with pristine radial structure were drilled to produce a powder for analysis.

Shell splinters from bivalves and powders from belemnites (300 to 600 µg) were flushed with helium, and reacted with phosphoric acid in sealed borosilicate Labco vials. The CO_2 generated was analysed for $\delta^{18}O$ and $\delta^{13}C$, following the procedures described in

Ullmann et al. (2013a), using the IsoPrime mass spectrometer at the IGN. Isotope ratios ($^{13}C/^{12}C$ and $^{18}O/^{16}O$) of the samples and laboratory working standards are measured against a CO_2 reference gas. The long-term precision (2 s.d.) for the isotope laboratories in Copenhagen is better than 0.1 ‰ for $\delta^{13}C$ and better than 0.2 ‰ for $\delta^{18}O$ based on the primary in-house reference material LEO (Carrara marble; $\delta^{13}C$ = +1.96 ‰ V-PDB, $\delta^{18}O$ = -1.93 ‰ V-PDB). This in-house standard had previously been calibrated against the international standards NBS 18 (Fen carbonatite; $\delta^{13}C$ = -5.014 ‰ V-PDB, $\delta^{18}O$ = -23.2 ‰ V-PDB) and NBS-19 (Carrara marble; $\delta^{13}C$ = +1.95 ‰ V-PDB, $\delta^{18}O$ = -2.20 ‰ V-PDB). Accuracy of the measurements was periodically controlled by measuring these international standards as well as other laboratory standards FUB CAM (Carrara marble; $\delta^{13}C$ = +2.42 ‰ V-PDB, $\delta^{18}O$ = -2.03 ‰ V-PDB), FUB KKS (Kaiserstuhl carbonatite; $\delta^{13}C$ = -5.75 ‰ V-PDB, $\delta^{18}O$ = -22.40 ‰ V-PDB) and FUB LM (Laaser marble; $\delta^{13}C$ = +1.51 ‰ V-PDB, $\delta^{18}O$ = -5.17 ‰ V-PDB) as unknowns. Carbon- and oxygen-isotope results were corrected and calibrated against V-PDB and are reported in the standard ‰-notation (Table 1 in auxiliary materials).

Mg/Ca, Sr/Ca, and Mn/Ca ratios for the studied samples were determined at the University of Copenhagen (Denmark) using a Perkin Elmer Optima 7000 DV ICP-OES adopting methodology outlined in Ullmann et al. (2013a). Sample residues from mass spectrometric analyses were transferred into 15 mL centrifuge tubes and diluted with 2 % HNO_3 to achieve a nominal concentration of 25 µg/g Ca in the solutions. These samples were analysed together with synthetic, matrix-matched, calibration solutions to allow for signal quantification and international standard materials JDo-1 and JL-1 for control of accuracy and precision. In order to account for contaminants in the phosphoric acid used for mass spectrometry, an aliquot of H_3PO_4 used for each isotope run of 45 samples was checked for Ca, Mg, Sr and Mn concentrations. Using known dilution factors of the mass spectrometric residues, these acid contributions to the elements of interest were then subtracted from the raw analytical data. Acid contributions were typically lower than 6 µmol/mol for Mn/Ca and 0.5 µmol/mol for Sr/Ca. Acid contributions could be significant for Mg/Ca (but almost always less than 25 % of the measured value), making the Mg/Ca data somewhat less certain than suggested by reproducibility of international reference materials alone. 2 s.d. reproducibility of the reference materials in the relevant time period was better than 3 % for Mg/Ca and Sr/Ca in JDo-1 and JLs-1 and better than ± 6 µmol/mol for Mn/Ca in JDo-1 and JLs-1, converting to a reproducibility of better than 3 % in JDo-1 and better than 8 % in JLs-1 due to the much lower Mn/Ca ratio of the latter standard. We therefore take a 2 s.d. reproducibility of 3 % as a

reasonable estimate of analytical quality for all determined ratios which are well above (50 times or more) the quantification limit of the instrument. Average equivalent quantification limits (10 s.d. of the baseline variability) for the analyses were < 0.4 mmol/mol for Ca, < 0.2 mmol/mol for Mg/Ca, < 2 µmol/mol for Sr/Ca and < 5 µmol/mol for Mn/Ca.

4. Results

Ultrastructural observations of the fossil shell materials using scanning electron microscopy (SEM) reveal varying degrees of textural preservation (Fig. 4). For a multitude of fossil *Gryphaea*, SEM imagery reveals shell structures typical of well-preserved oysters, notably thin sheets subdivided into fanned bundles of elongate single crystals, also known from the foliate layers of their modern counterparts (Ullmann et al., 2013b). A continuum towards progressively diagenetically overprinted shell structures is also observed, where first the definition of the single crystal units becomes lost, and then the integrity of crystal superunits and sheets. These effects are notable in the samples from the Hebrides at Ardnish (Fig. 4d), but even more pronounced in samples from Boreraig (Fig. 4e), where alteration in the thermal aureole of the Beinn an Dubhaich granite is likely (see section 5.1. below).

A substantial depletion of ^{18}O in the shell layers that show fusion and loss of fine textural detail is indicated, with specimens imaged in Fig. 4e and 4f yielding $\delta^{18}O$ values of -8.1 ‰ and -10.3 ‰, respectively. Intermediate values for samples from the specimen imaged in Figure 4d (-3.5 and -6.0 ‰) are found, whereas all of the specimens from Figs. 4a-c yield $\delta^{18}O$ values > -2 ‰. A direct comparison of shell ultrastructure with isotopic information is not possible, because not all analysed fossils could be studied using the SEM and isotopic measurements could not be made on the exact same shell fragment used for SEM observation. SEM data can therefore only be used for general guidance relating to shell preservation in the different studied sections.

Carbon- and oxygen-isotope ratios show the heterogeneity typical of macrofossils from the British Isles (cf. Bailey et al., 2003; Dera et al., 2011; Korte et al., 2015), spanning a range of ~2 ‰ or more in both isotopic systems for any given stratigraphic datum (Fig. 5). Carbon-isotope ratios are characterized by a substantial increase in the lowermost Hettangian strata, which reach a sharp peak at values as high as +5 ‰ in the *tilmanni* Zone, and reducing subsequently to < +3 ‰ into the *planorbis* Zone. The $\delta^{13}C$ values of +3 ‰ are not again

surpassed in the Hettangian strata in which carbon-isotope ratios show a further gentle decline to average values of ~ +1.5 ‰ in the *angulata* Zone at the top of the Hettangian. The lowermost Sinemurian strata, and possibly the uppermost Hettangian strata evidence a substantial increase in $\delta^{13}C$, with some values approaching +4 ‰ in the *bucklandi* Zone and exceeding this slightly in the *semicostatum* and *turneri* zones, almost reaching values as high as in the lowermost Hettangian. We stress that the ranges in values described above include an internal shell heterogeneity that relates neither to analytical uncertainty nor to diagenesis (discussed further in section 5 below). Therefore these values, although extremes, still have real palaeoenvironmental meaning, for example in relation to seasonal conditions in the water column. Through the studied interval the carbon-isotope ratios appear to be characterized by systematic minor (sub-permil) fluctuations at the ammonite zone to subzone time scale (Fig. 5). These minor fluctuations are particularly evident in the *bucklandi* and *semicostatum* zones, where data density is highest.

Oxygen-isotope ratios of the shell material are comparatively positive in the lowermost Hettangian strata, reaching values almost as high as +2 ‰ (Figs. 5, 6). A strong decrease from this maximum is observed into the *planorbis* Zone, where $\delta^{18}O$ values generally fall into the range from -1 to -2 ‰. Through the remainder of the studied interval most data fall into this range with some minor positive and negative deviations (Fig. 5). A mild (sub-permil) overall decrease in $\delta^{18}O$ from the Hettangian *planorbis* Zone into the Sinemurian *turneri* Zone can be gleaned from the data (Fig. 6). Generally, however, oxygen-isotope ratios excluding samples from the *tilmanni* Zone show much less dynamic evolution than equivalent carbon-isotope ratios.

5. Discussion

5.1. Diagenetic and hydrothermal alteration

Diagenesis-related ^{18}O depletion in LMC calcite is commonly more severe than ^{13}C depletion, and is related to interaction of calcite with ^{18}O-depleted fluids or elevated temperatures during alteration (e.g. Brand and Veizer, 1981; Al-Aasm and Veizer, 1986a; Swart, 2015; Ullmann and Korte, 2015). In contrast to the clear separation of $\delta^{18}O$ values, with isotopic ratios as low as nearly -20 ‰ recorded at Boreraig, $\delta^{13}C$ values of the Boreraig, Ardnish and Hallaig Waterfall samples overlap entirely (Fig. 7) and are comparable to

reported results from biogenic carbonate of this age elsewhere (Jenkyns et al., 2002). The contrasting isotopic response suggests that alteration around Skye is caused by interaction of calcite with hot fluids related to the Paleogene igneous activity in the region, particularly intrusion of the Beinn an Dubhaich granite. Previous work on the metamorphic aureole of the Beinn an Dubhaich granite has already demonstrated the occurrence of depleted oxygen-isotope values in hydrothermally altered silicate minerals (Taylor and Forester, 1971; Forester and Taylor, 1977) and carbonates (Holness and Fallick, 1997), but in both cases from closer to the pluton itself compared to the results reported here. Evidently, the oxygen-isotope values of macrofossils are quite sensitive indictors of alteration in hydrothermal systems.

While the nature and origin of these fluids are not resolvable by the present dataset, it is very probable that temperature-related depletion of ^{18}O at Boreraig and, to some lesser degree, at the more distant location of Ardnish, is responsible for the majority of the oxygen isotope signal. Presently, annually averaged rainwater $\delta^{18}O$ on the west coast of the UK is between -5 and -10 ‰ V-SMOW (Araguás-Araguás et al., 2000; Tyler et al., 2016). Considering the expected warm climate at the time of Beinn an Dubhaich emplacement (e.g. Barnet et al., 2019), and a plate tectonic arrangement not unlike that of today in the relevant region, values more negative than today and therefore groundwater $\delta^{18}O$ more negative than -8 ‰ are not particularly expected. Using the oxygen isotope thermometer of O'Neil et al. (1969) for high-temperature calcite formation and -20 ‰ as a first order assumption for diagenetic calcite in isotopic equilibrium, formation temperatures can be estimated. Resulting temperatures during recrystallization are approximately 160°C if the fluid was seawater-like (-1 ‰ V-SMOW; e.g. Suan et al., 2008) and 80°C if the fluid was derived from groundwater (-8 ‰ V-SMOW) (see also Ullmann and Korte, 2015 and their figure 8a for discussion).

A measurable temperature dependence on fractionation exists also for carbon-isotope ratios between dissolved bicarbonate and calcite, and amounts to approximately 0.06 ‰ per degree centigrade at a temperature of 20°C (Emrich et al., 1970). The carbon-isotope signatures of fossils from the three Hebridean localities are indistinguishable, and a temperature effect accidentally perfectly counterbalanced by addition to the diagenetic fluids of appropriate quantities of isotopically heavy carbon can be excluded as highly unlikely. Carbonates more closely related to Beinn an Dubhaich intrusion fluids typically show $\delta^{13}C$ values of -5 to 0 ‰ (Holness and Fallick, 1997), suggesting that fluids involved during fossil recrystallization did not carry enough isotopically distinct carbon to overprint the primary

$\delta^{13}C$ signatures at these locations. These observations in conjunction therefore make it probable that partial overprint of by fluids took place at the lower end of the range of temperature possibilities given by oxygen-isotope data, involving fluids buffered in their C isotope composition by locally derived carbonates.

Manganese is a transition metal that is commonly used as a sensitive indicator for carbonate diagenesis (e.g., Brand and Veizer, 1980, Al-Aasm and Veizer, 1986b, Ullmann and Korte, 2015). However, in the dataset from Scotland the relationship between Mn/Ca and $\delta^{18}O$ is too weak to discriminate strongly between isotopically depleted and near primary samples. The r^2 for Boreraig is 0.00 ($r = -0.04$; $p = 0.66$, $n = 131$) and the r^2 for Ardnish is 0.11 ($r = -0.34$; $p < 10^{-4}$, $n = 130$) (see also Fig. 6). Therefore Mn content is of little use for removing the alteration signal in this case. Samples with Mn/Ca ratios > 0.5 mmol/mol, however, are removed from the compiled stratigraphic plots. Such high Mn/Ca ratios are unknown from modern oysters (Almeida et al., 1998; Ullmann et al., 2013b) and it is probable therefore that fossil samples flagged in this way have undergone significant alteration.

The Sr/Ca ratio of biogenic calcite commonly decreases in concert with post-depositional alteration (e.g., Brand and Veizer, 1980, Al-Aasm and Veizer, 1986b, Ullmann and Korte, 2015). Fossil ostreoids, which comprise the largest part of the present dataset, however, show very low primary Sr concentrations when compared to other fossil groups (Ullmann et al., 2013c). Such low Sr/Ca ratios may be very close to Sr/Ca ratios of diagenetic carbonate, especially during the Sinemurian, which is interpreted to be a time of relatively low seawater Sr/Ca ratios (Ullmann et al., 2013c). Correlations of Sr/Ca ratios with Mn/Ca, $\delta^{13}C$ and $\delta^{18}O$ values are thus in this particular instance not capable of robustly separating well-preserved from altered samples.

5.2. Isotope stratigraphy, carbon cycle, and palaeotemperature

The relationships between changes to the principal parameters in the carbon cycle, such as the burial flux of carbonate carbon and organic carbon, silicate weathering intensity, atmospheric carbon dioxide content, and palaeotemperature, are matters of keen interest, especially at and after times of major environmental change and mass extinction (Kump 2018), but with little hard evidence for the time interval under scrutiny here. During Mesozoic Oceanic Anoxic Events (OAE's), such as definitively occurred in the Toarcian (the T-OAE;

Jenkyns 1988), and possibly also at the Triassic-Jurassic boundary (e.g. Hallam, 1990; van de Schootbrugge et al., 2008, 2013; Jost et al., 2017), it has been postulated that positive carbon-isotope excursions (+ve CIE's) correspond to relatively enhanced organic carbon-burial flux, low atmospheric CO_2, and cold palaeotemperatures, whereas negative carbon-isotope excursions (-ve CIE's) correspond to relatively high flux of light carbon into the ocean-atmosphere system, high atmospheric CO_2, and high palaeotemperatures (e.g. Jenkyns, 2010; Robinson et al., 2016).

Recent work on T-OAE palaeotemperature, based on oxygen-isotopes of Iberian brachiopods, also suggests that the effectiveness of the silicate weathering carbon sink may have reduced in intensity through the event, allowing warm temperatures to strongly persist well past the peak of the characteristic negative CIE, and complicating interpretation of the link between carbon-isotope ratios and atmospheric CO_2 (Ullmann et al., 2020 in review). Although it is clear that further Hettangian–Sinemurian datasets are needed, of comparable size and stratigraphic resolution, and from other regions of the globe, the new data presented here unambiguously show a divergence between evolving carbon-isotope and oxygen-isotope values in the seaway from the late Hettangian to the Sinemurian (Figs 5, 6). Below we briefly consider the significance of this observation.

The relatively positive carbon-isotope values reach a peak at the top of the lower Sinemurian (*semicostatum* and *turneri* zones). A similar pattern was shown but in much lower resolution in the macrofossil data of Jenkyns et al. (2002) for the Wessex and Cleveland Basins, UK. Data from the Paris Basin, France (Nori and Lathuilière, 2003), also fit into the same overall trends. Unusually positive carbon-isotope values are further evident episodically in bulk organic carbon-isotope records from the middle to upper parts of the Sinemurian of the same NW European region (van de Schootbrugge et al., 2005, 2019; Riding et al., 2013; Jenkyns and Weedon, 2013; Peti et al., 2017; Schöllhorn et al., 2020; Storm et al., 2020), and from western Canada (Porter et al., 2014).

Whether the subzone-scale fluctuations in carbon-isotope values are a phenomenon of the regional or global carbon-cycles, or result from localised environmental factors, is still to be determined with confidence as, for example, discussed most recently by Schöllhorn et al. (2020) and Storm et al. (2020). The most positive carbon-isotope values of the Jenkyns and Weedon (2013) bulk organic carbon curve occur in the upper (*birchi*) subzone of the *turneri*

Zone, in contrast to the pattern observed here where the peak appears to be in the lower (*brooki*) subzone. The Jenkyns and Weedon (2013) record is derived from southern England, whereas our record for the same interval comes from northern Scotland, and so it is possible that the difference stems from uncertainty in biostratigraphic correlation as opposed to real difference in timing between the two locations.

Schöllhorn et al. (2020) argue that at least some of carbon-isotope cycles at the scale of ammonite subzones seen in their dataset form S England are due to mixing of terrestrial and marine organic components, and are largely eliminated by using pyrolysis data to perform a correction (specifically relating to hydrogen index (HI) values; cf. Suan et al., 2015). A high-resolution carbon-isotope curve from bulk-organic carbon through the Lower Jurassic of the Llanbedr (Mochras Farm) borehole in N Wales (Storm et al., 2020) also shows subzone-scale cyclicity in the $\delta^{13}C_{org}$ values which are there ascribed to 405 kyr eccentricity palaeoclimatic forcing of the carbon-cycle on at least a regional scale. In the case of the Mochras dataset, however, some of the variation of hydrogen index is interpreted to be from oxidation of marine organic matter in the water column, in addition to, or instead of, admixture of terrestrial organic matter (Storm et al., 2020), and so raising questions about the effectiveness of a $\delta^{13}C_{org}$ 'correction' based on pyrolysis data beyond other issues already identified (see discussion in Schöllhorn et al. (2020).

The trends in oxygen-isotope values reported here are not evident in the Jenkyns et al. (2002) dataset because of the relative sparsity of points and comparatively noisy signal in the earlier compilation. As noted above in Section 4 and shown in Figure 6, there is an overall slight trend in the new dataset towards more negative values from the lower Hettangian through to the top part of the lower Sinemurian. Oxygen-isotope values of invertebrate shells can be influenced by a significant number of variables, of which temperature is the most prominently discussed, but which also include biological ('vital') effects, contributions to the watermass from freshwater input (-ve shift), watermass changes from evaporation (+ve shift), or change in continental ice volume (e.g., with respect to the Laurasian Seaway and western Tethys, see Rosales et al., 2004; Dera et al., 2011; Dera and Donnadieu, 2012; Korte et al., 2015; Gomez et al., 2016; Ruebsam et al., 2019; Baghli et al., 2020). Given the mix of fossil taxa analysed here – predominantly ostreid bivalves – it is unfeasible to argue that the overall trends represent a purely biological artefact.

Change in watermass isotopic composition through change in the evaporation/precipitation balance is more difficult to rule out as a mechanism, but appears unlikely; all analysed fossils are part of assemblages that contain unambiguously fully marine organisms such as ammonites, brachiopods, and crinoids. The only exception to this observation is for the dataset of Korte et al. (2009) from the basal Hettangian *tilmanni* Zone of the Bristol Channel Basin, where the salinity has been previously suggested to have been, at least episodically, divergent from normal marine (Hallam and El-Sharaawy, 1982); in counter-argument the correlative limestone of the Lilstock Formation in the Wessex Basin, S England, contains typically stenohaline forms (such as corals) and also displays prominently a positive carbon isotope excursion typical of the middle *tilmanni* Zone, thus arguing against deviation from open marine conditions (Hesselbo and Jenkyns, 1995; Hesselbo et al., 2004; Korte et al., 2009).

A further factor to be considered is that the oxygen isotope (along with carbon isotope) values may signify stratified water masses with isotopic compositions determined by low density surface water strongly influenced by freshwater sources (e.g. Fleet et al., 1987; Wignall and Hallam, 1991; Dera and Donnadieu, 2012; Jenkyns and Weedon, 2013). Such conditions might be expected especially at the times of black shale deposition. Whilst freshened and stratified watermasses may indeed have been important at times, such effects cannot explain the long-term trends reported here because of the diverse nature of the benthos samples which come from a variety of environments, most of which are characterised by bioturbated, well-oxygenated sea-floor, and therefore well mixed conditions. Certainly, there is no overall trend to more strongly stratified conditions with time. Given that the younger parts of the new record come from the more northerly localities (Fig. 5) another possible factor to consider is an increased northward contribution of meteoric water to seawater $\delta^{18}O$ values (cf. Rosales et al., 2004); although this cannot be categorically ruled out as an explanation of the data, there are no abrupt jumps between geographically separate datasets, and so such an artefact also seems unlikely.

Drawing the discussion together, the isotopic values measured are multifactorial in origin, but we hypothesise that the carbon-isotope trends are at least super-regional in nature, and potentially global, and that the oxygen-isotope trends represent predominantly changing bottom-water seawater palaeotemperatures though time. On this basis we conclude that any atmospheric carbon-dioxide drawdown effect on global palaeotemperatures from carbon

burial, as suggested by progressively increasing $\delta^{13}C_{carb}$ and $\delta^{13}C_{org}$ values into the middle Sinemurian, was more than counterbalanced by a reduction in the global weathering sink for CO_2 (e.g. Ullmann et al, 2020 in review), or else counterbalanced in the seaway by regional processes that led to significantly warmer bottom water temperatures. Whether the relationships observed here are representative of global trends, or relate exclusively to seaway dynamics, is presently unknown, and will require similar datasets from other locations in order to determine. Clay mineral data from southern England (Deconinck et al., 2003) show a clear trend towards increased kaolinite/illite ratios through the Hettangian and Sinemurian, compatible with a gradual hinterland warming and humidity over the same interval. The same trend is documented over a parallel but stratigraphically extended record also from the south of England, where, additionally, chemical index of alteration (CIA) data support enhanced weathering in increasingly warm and humid environments (Schöllhorn et al., 2020).

6. Conclusions

Carbon- and oxygen- isotope values from the low Mg calcite hard parts of selected marine molluscs and brachiopods from a number of UK locations, show temporal trends through the Hettangian to top lower Sinemurian. Following extreme positive $\delta^{13}C_{carb}$ values immediately above the Triassic-Jurassic boundary, the Hettangian is characterised by sustained relatively negative values, before a progressive return to heavy $\delta^{13}C_{carb}$ values through the lower Sinemurian. Oxygen-isotope values from the same fossils show a very slight progressive change to more negative values over the top Hettangian through lower Sinemurian interval. If carbon-isotope values relate principally to organic-carbon burial flux, then the implied palaeotemperatures from the late Hettangian to mid Sinemurian likely reflect palaeoceanographic changes in the seaway, rather than a response to global carbon-dioxide drawdown predicted from the inferred organic carbon burial.

Acknowledgements

We thank the Danish Council for Independent Research–Natural Sciences (project 09-072715 and DFF-7014-00142, and the Carlsberg Foundation (project nr 2011-01-0737) for contributions to financing this project provided for CK. We acknowledge M. Jelby and B. Petersen (both Copenhagen) for preparing some samples and assistance with isotope analyses, respectively. SPH and CVU acknowledge funding from NERC (NE/N018508/1); CVU

acknowledges support from the Leopoldina – German National Academy of Sciences (grant no. LPDS 2014-08). This is a contribution to the JET project. This manuscript benefitted greatly from critical comments from guest editor Tom Algeo, Pierre Pellenard, and an anonymous reviewer.

Declaration of interests

The authors declare that they have no known competing financial interests or personal relationships that could have appeared to influence the work reported in this paper.

References

Al-Aasm, I.S., Veizer, J., 1986a. Diagenetic stabilization of aragonite and low-Mg calcite, I. trace elements in rudists. Journal of Sedimentary Petrology 56 (1), 138–152.

Al-Aasm, I.S., Veizer, J., 1986b. Diagenetic stabilization of aragonite and low-Mg calcite, II. Stable isotopes in rudists. Journal of Sedimentary Petrology 56 (6), 763–770.

Almeida, M.J., Machado, J., Moura, G., Azevedo, M., Coimbra, J., 1998. Temporal and local variations in biochemical composition of *Crassostrea gigas* shells. Journal of Sea Research 40, 233-249.

Al-Suwaidi, A.H., Steuber, T., Suarez, M.B., 2016. The Triassic–Jurassic boundary event from an equatorial carbonate platform (Ghalilah Formation, United Arab Emirates). Journal of the Geological Society 173, 949–953.

Anderson, T.F., Arthur, M.A., 1983. Stable isotopes of oxygen and carbon and their application to sedimentologic and environmental problems. In Stable Isotopes in Sedimentary Geology, SEPM Short Course Notes No. 10, 1–151. Tulsa, Oklahoma: Society of Economic Palaeontologists and Mineralogists.

Araguás-Araguás, L., Froehlich, K., Rozanski, K., 2000. Deuterium and oxygen-18 isotope composition of precipitation and atmospheric moisture. Hydrological Processes 14, 1341–1355.

Bachan, A., van de Schootbrugge, B., Fiebig, J., McRoberts, C. A., Ciarapica, G., Payne, J. L., 2012. Carbon cycle dynamics following the end-Triassic mass extinction: Constraints from paired $\delta^{13}C_{carb}$ and $\delta^{13}C_{org}$ records. Geochemistry, Geophysics, Geosystems 13, Q09008.

Baghli, H., Mattioli, E., Spangenberg, J.E., Bensalah, M., Arnaud-Godet, F., Pittet, B., Suan, G., 2020. Early Jurassic climatic trends in the south-Tethyan margin. Gondwana Research, in press.

Bailey, T.R., Rosenthal, Y., McArthur, J.M., van de Schootbrugge, B., Thirlwall, M.F., 2003. Paleoceanographic changes of the late Pliensbachian–Early Toarcian interval: a possible link to the genesis of an oceanic anoxic event. Earth Planet. Sci. Lett. 212, 307–320.

Barnet J, Littler K, Westerhold T, Kroon D, Leng M, Bailey I, Rohl U, Zachos J., 2019. A high-fidelity benthic stable isotope record of Late Cretaceous–Early Eocene climate change and carbon-cycling. Paleoceanography and Paleoclimatology 34, 672–691.

Bartolini, A., Guex, J., Spangenberg, J., Schoene, B., Taylor, D., Schaltegger, U., Atudorei, V., 2012. Disentangling the Hettangian carbon isotope record: Implications for the aftermath of the end-Triassic mass extinction. Geochemistry, Geophysics, Geosystems 13, Q01007.

Bjerrum, C.J., Surlyk, F., Callomon, J.H., Singerland, R.L., 2001. Numerical paleoceanographic study of the Early Jurassic transcontinental Laurasian Seaway. Paleoceanography 16, 390–404.

Bloos, G., Page, K.N., 2002. Global Stratotype Section and Point for base of the Sinemurian Stage (Lower Jurassic). Episodes 25, 22–28.

Brand, U., Veizer, J., 1980. Chemical diagenesis of a multicomponent carbonate system -1: trace elements. Journal of Sedimentary Petrology 50 (4), 1219–1236.

Brand, U., Veizer, J., 1981. Chemical diagenesis of a multicomponent carbonate system -2: stable isotopes. Journal of Sedimentary Petrology 51 (3), 987–997.

Clémence, M.-E., Bartolini, A., Gardin, S., Paris, G., Beaumont, V., Page, K.N., 2010. Early Hettangian benthic-planktonic coupling at Doniford (SW England): Palaeoenvironmental implications for the aftermath of the end-Triassic crisis. Palaeogeography, Palaeoclimatology, Palaeoecology 29, 102–115.

Cochran, J.K., Kallenberg, K., Landman, N.H., Harries, P.J., Weinreb, D., Turekian, K.K., Beck, A.J., Cobban, W.A., 2010. Effect of diagenesis on the Sr, O, and C isotope composition of Late Cretaceous mollusks from the Western Interior Seaway of North America. American Journal of Science 310, 69–88.

Coward, M. P., Dewey, J. F., Mange, M., Hempton, M., Holroyd, J., 2003. Tectonic Evolution. In: Evans, D., Graham, C., Armour, A., Bathurst, P. (Eds.), The

Millennium Atlas: Petroleum Geology of The Central and Northern North Sea. Geological Society Publishing House, p.17–33.

Cox, B.M., Sumbler, M.G., Ivimey-Cook, H.C., 1999. A formational framework of the Lower Jurassic of England and Wales. British Geological Survey Research Report, RR/99/01.

Damborenea S.E., 2002. Jurassic evolution of Southern Hemisphere marine palaeobiogeographic units based on benthonic bivalves. Geobios 35, Mém. Spec. 24, 51–71.

Deconinck, J.-F., Hesselbo, S.P., Debuisser, N., Averbuch, O., Baudin, F., Bessa, J., 2003. Environmental controls on clay mineralogy of an early Jurassic mudrock (Blue Lias Formation, southern England). Int. J. Earth Sci. 92, 255–266.

Deenen, M.H.L., Ruhl, M., Bonis, N.R., Krijgsman, W., Kuerschner, W.M., Reitsma, M., van Bergen, M.J., 2010. A new chronology for the end-Triassic mass extinction. Earth and Planetary Science Letters 291, 113–125.

Dera, G., Pellenard, P., Neige, P., Deconinck, J.-F., Pucéat, E., Dommergues, J.-L., 2009. Distribution of clay minerals in Early Jurassic Peritethyan seas: Palaeoclimatic significance from multiproxy comparisons. Palaeogeography, Palaeoclimatology, Palaeoecology 271, 39–51.

Dera, G., Brigaud, B., Monna, F., Laffont, R., Pucéat, E., Deconinck, J.-F., Pellenard, P., Joachimski, M.M., Durlet, C., 2011. Climatic ups and downs in a disturbed Jurassic world. Geology 39, 215–218.

Dera, G., Donnadieu, Y., 2012. Modeling evidences for global warming, Arctic seawater freshening, and sluggish oceanic circulation during the Early Toarcian anoxic event. Paleoceanography 27, 1–15.

Emrich, K., Ehhalt, D.H., Vigel, J.C., 1970. Carbon isotope fractionation during the precipitation of calcium carbonate. Earth and Planetary Science Letters 8, 363–371.

Fleet, A.J., Clayton, C.J., Jenkyns, H.C., Parkinson, D.N., 1987. Liassic source-rock deposition in western Europe. In: Brooks, J., Glennie, K. (Eds.), Petroleum Geology of north-west Europe, 1, Graham and Trotman, 59–70.

Forester, R.W., Taylor, H.P., 1977. $^{18}O/^{16}O$, D/H, and $^{13}C/^{12}C$ studies of the Tertiary igneous complex of Skye, Scotland. American Journal of Science 277, 136–177.

Gradstein, F.M., Ogg, J.G., Schmitz, M. and Ogg, G. eds., 2012. The Geologic Time Scale 2012. Elsevier.

Gómez, J.J., Comas-Rengifo, M.J., Goy, A., 2016. Palaeoclimatic oscillations in the Pliensbachian (Early Jurassic) of the Asturian Basin (Northern Spain). Clim. Past Discuss. 12, 1199–1214.

Hallam, A., 1959. Stratigraphy of the Broadford Beds of Skye, Raasay and Applecross. Proceedings of the Yorkshire Geological Society 32, 165–84.

Hallam, A., 1990. The end-Triassic mass extinction event. Geol. Soc. Am. Spec. Pap. 247, 577–584.

Hallam, A., El-Sharaawy, Z., 1982. Salinity reduction of the end-Triassic sea from the Alpine region into northwestern Europe. Lethaia 15, 169–178.

Hesselbo, S.P., Jenkyns, H.C., 1995. A comparison of the Hettangian to Bajocian successions of Dorset and Yorkshire. In: Taylor, P.D. (Ed.), Field Geology of the British Jurassic, Geological Society of London, p. 105–150.

Hesselbo, S.P., Coe, A.L., 2000. Jurassic sequences of the Hebrides Basin, Isle of Skye, Scotland. In: Graham J.R., Ryan, A. (Eds), Field Trip Guidebook, International Association of Sedimentologists Meeting, Dublin, 2000, p. 41–58. University of Dublin, Dublin.

Hesselbo, S.P., Oates, M.J., Jenkyns, H.C., 1998. The lower Lias Group of the Hebrides Basin. Scottish Journal of Geology 34, 23–60.

Hesselbo, S.P., Robinson, S.A., Surlyk, F., Piasecki, S., 2002. Terrestrial and marine extinction at the Triassic-Jurassic boundary synchronized with major carbon-cycle perturbation: a link to initiation of massive volcanism? Geology 30, 251–254.

Hesselbo, S.P., Robinson, S.A., Surlyk, F., 2004. Sea-level change and facies development across potential Triassic–Jurassic boundary horizons, south west Britain. Journal of the Geological Society London 161, 365–379.

Hodges P., 1986. The Lower Lias (Lower Jurassic) of the Bridgend area, South Wales. Proc. Geol. Assoc. 97, 237–242.

Hoersch, A.L., 1981. Progressive metamorphism of the chert-bearing Durness limestone in the Beinn an Dubhaich aureole, Isle of Skye, Scotland: a re-examination. American Mineralogist, 66, 491–506.

Holness, M.B., 1997. Fluid flow paths and mechanisms of fluid infiltration in carbonatesduring contact metamorphism: the Beinn an Dubhaich aureole, Skye. Journal of Metamorphic Geology, 15, 59–70.

Holness, M.B., Fallick, A.E., 1997. Palæohydrology of the calcsilicate aureole of the Beinn an Dubhaich granite, Skye, Scotland: a stable isotopic study. Journal of Metamorphic Geology, 15, 71–83.

Hüsing, S.K., Beniest, A., van der Boon, A., Abels, H.A., Deenen, M.H.L., Ruhl, M., Krijgsman, W., 2014. Astronomically-calibrated magnetostratigraphy of the Lower Jurassic marine successions at St. Audrie's Bay and East Quantoxhead (Hettangian-Sinemurian; Somerset, UK). Palaeogeography, Palaeoclimatology, Palaeoecology 403, 43–56.

Jenkyns, H.C., 1988. The Early Toarcian (Jurassic) Anoxic Event: stratigraphic, sedimentary and geochemical evidence. Am. J. Sci. 288, 101–151.

Jenkyns, H.C., 2010. Geochemistry of oceanic anoxic events. Geochem. Geophys. Geosys. 11, Q03004.

Jenkyns, H.C., Weedon, G.P., 2013. Chemostratigraphy ($CaCO_3$, TOC, $\delta^{13}C_{org}$) of Sinemurian (Lower Jurassic) black shales from the Wessex Basin, Dorset and palaeoenvironmental implications. Newslett. Stratigr. 46, 1–21.

Jenkyns, H.C., Jones, C.E., Gröcke, D.R., Hesselbo, S.P., Parkinson, D.N., 2002. Chemostratigraphy of the Jurassic System: applications, limitations and implications for palaeoceanography. Journal of the Geological Society, London 159, 351–378.

Jost, A.B., Bachan, A., van deSchootbrugge, B., Lau, K.V., Weaver, K.L., Maher, K., Payne, J.L., 2017. Uranium isotope evidence for anexpansion of marine anoxia during theend-Triassic extinction. Geochem.Geophys. Geosyst. 18, 3093–3108.

Korte, C., Hesselbo, S.P., 2011. Shallow-marine carbon- and oxygen-isotope and elemental records indicate icehouse-greenhouse cycles during the Early Jurassic. Paleoceanography 26, PA4219.

Korte, C., Hesselbo, S.P., Jenkyns, H.C., Rickaby, R.E.M., Spötl, C., 2009. Palaeoenvironmental significance of carbon- and oxygen-isotope stratigraphy of marine Triassic–Jurassic boundary sections in SW Britain. Journal of the Geological Society, London 166, p. 431–445.

Korte, C., Hesselbo, S.P., Ullmann, C.V., Dietl, G., Ruhl, M., Schweigert, G., Thibault, N., 2015. Jurassic climate mode governed by ocean gateway. Nature Communications 6:10015. doi: 10.1038/ncomms10015.

Korte, C., Ruhl, M., Pálfy, J., Ullmann, C.V., Hesselbo, S.P., 2019. Chemostratigraphy across the Triassic–Jurassic boundary. In: Sial, A.N., Gaucher, C., Ramkumar, M., Ferreira, V.P. (Eds.), Chemostratigraphy Across Major Chronological Boundaries, Geophysical

Monograph 240. The American Geophysical Union; John Wiley & Sons, Inc. AGU Books. p. 185–210.

Kump, L.R., 2018. Prolonged Late Permian–Early Triassic hyperthermal: failure of climate regulation? Philosophical Transactions of the Royal Society A 376.

Marzoli, A., Renne, P.R., Piccirillo, E.M., Ernesto, M., Bellieni, G., De Min, A., 1999. Extensive 200-million-year-old continental flood basalts of the Central Atlantic Magmatic Province. Science 284(5414), 616–618.

Morton N., Hudson J. D., 1995. Field guide to the Jurassic of the Isles of Raasay and Skye, Inner Hebrides, NW Scotland. In: Taylor, P.D. (Ed.) Field Geology of the British Jurassic, pp. 209–280. London: The Geological Society.

McHone, J.G., 1996. Broad-terrane Jurassic flood basalts across northeastern North America. Geology 24, 319–322.

Nori, L., Lathuilière, B., 2003. Form and environment of *Gryphaea arcuata*. Lethaia 36, 83–96.

O'Neil, J.R., Clayton, R.N., Mayeda, T.K., 1969. Oxygen isotope fractionation in divalent metal carbonates. The Journal of Chemical Physics 51 (12), 5547–5558.

Page, K.N., 1992. The sequence of ammonite correlated horizons in the British Sinemurian (Lower Jurassic). Newsletters on Stratigraphy 27, 129–156.

Page, K.N., 1994. On the sequence of ammonite correlated chronostratigraphical horizons in the British Sinemurian (Lower Jurassic). In: Proceedings of the 3rd International Symposium on Jurassic Stratigraphy, Poitiers 1991. Geobios, Mém. Spécial 17, 369–379.

Page, K.N., 2005. The Hettangian ammonite faunas of the West Somerset coast (south west England) and their significance for the correlation of the candidate GSSP (Global Stratotype and Point) for the base of the Jurassic System at St. Audries Bay. In: Hanzo, M. (coord.), Colloque Hettangien à Hettange, de la science au patrimoine, Hettange, 1-3 avril 2005: 15-19. Unversité Henri Poncaré, Nancy.

Page, K.N., 2010. Stratigraphical Framework. In: Lord, A.R., Davis, P.G. (Eds.) Fossils from the Lower Lias of the Dorset Coast, Palaeontological Association Field Guide to Fossils, 13, 33–53.

Pálfy, J., Demeny, A., Haas, J., Hetenyi, M., Orchard, M.J., Veto, I., 2001. Carbon isotope anomaly and other geochemical changes at the Triassic–Jurassic boundary from a marine section in Hungary. Geology 29, 1047–1050.

Palmer, C.P., 1972. The Lower Lias (Lower Jurassic) between Watchet and Lilstock in North Somerset (United Kingdom). Newsletters on Stratigraphy 2, 1–30.

Peti, L., Thibault, N., Clémence, M.-E., Korte, C., Dommergues, J.-L., Bougeault, C., Pellenard, P., Jelby, M.E., Ullmann, C.V., 2017. Sinemurian-Pliensbachian calcareous nannofossil biostratigraphy and organic carbon isotope stratigraphy in the Paris Basin: Calibration to the ammonite biozonation of NW Europe. Palaeogeography, Palaeoclimatology, Palaeoecology 468, 142–161.

Porter, S.J., Smith, P.L., Caruthers, A.H., Hou, P., Gröcke, D.R., Selby, D., 2014. New high resolution geochemistry of Lower Jurassic marine sections in western North America: A global positive carbon isotope excursion in the Sinemurian? Earth Planet. Sci. Lett., 397, 19–31.

Riding, J.B., Leng, M.L., Kender, S., Hesselbo, S.P., Feist-Burkhardt, S., 2013. Isotopic and palynological evidence for a new Early Jurassic environmental perturbation. Palaeogeography, Palaeoclimatology, Palaeoecology 374, 16–27.

Ruhl, M., Kürschner, W.M., Krystyn, L., 2009. Triassic–Jurassic organic carbon isotope stratigraphy of key sections in the western Tethys realm (Austria). Earth Planet. Sci. Lett. 281, 169–187.

Ruhl, M., Deenen, M.H.L., Abels, H.A., Bonis, N.R., Krijgsman, W., Kürschner, W.M., 2010. Astronomical constraints on the duration of the early Jurassic Hettangian stage and recovery rates following the end-Triassic mass extinction (St Audrie's Bay/East Quantoxhead, UK). Earth and Planetary Science Letters 295, 262–276.

Robinson, S.A., Heimhofer, U., Hesselbo, S.P. Petrizzo, M.R., 2017. State of the Science: Mesozoic climates and oceans – a tribute to Hugh Jenkyns and Helmut Weissert. Sedimentology 64, 1–15.

Rosales, I., Robles, S. Quesada, S. 2004. Elemental and oxygen isotope composition of Early Jurassic belemnites: salinity vs. temperature signals. Journal of Sedimentary Research 74, 342-354

Ruebsam, W., Mayer, B., Schwark, L., 2019. Cryosphere carbon dynamics control early Toarcian global warming and sea level evolution. Global and Planetary Change 172, 440–453.

Samtleben, C., Munnecke, A., Bickert, T., Pätzold, J., 2001. Shell succession, assemblage and species dependent effects on the C/O-isotopic composition of brachiopods – examples from the Silurian of Gotland. Chemical Geology 175, 61–107.

Schöllhorn, I., Adatte, T., Van de Schootbrugge, B., Houben, A., Charbonnier, G., Janssen, N., Föllmi, K.B. 2020. Climate and environmental response to the break-up of Pangea during the Early Jurassic (Hettangian-Pliensbachian); the Dorset coast (UK) revisited. Global and Planetary Change 185, 103096.

Sheppard, H.T., 2006. Sequence architecture of ancient rocky shorelines and their response to sea-level change: an Early Jurassic example from South Wales, UK. Journal of the Geological Society, London 163, 595–606.

Simms, M.J., Chidlaw, N., Morton, N., Page, K.N., 2004. British Lower Jurassic Stratigraphy, Geological Conservation Review Series, No. 30, Joint Nature Conservation Committee, Peterborough, 458 pp.

Stoker, M.S., Stewart, M.A., Shannon, P.M., Bjerager, M., Nielsen, T., Blischke, A., Hjelstuen, B.O., Gaina, C., Mcdermott, K., Ólavsdóttir, J., 2016. An overview of the Upper Palaeozoic-Mesozoic stratigraphy of the NE Atlantic region. Geological Society Special Publication 447, 11–68.

Storm, M.S., Hesselbo, S.P., Jenkyns, H.C., Ruhl, M., Ullmann, C.V., Xu, W., Leng, M.J., Riding, J.B., Gorbanenko, O., 2020. Orbital pacing and secular evolution of the Early Jurassic carbon cycle. Proc. Nat. Acad. Sci., in press.

Suan, G., Mattioli, E., Pittet, B., Mailliot, S., Lécuyer, C., 2008. Evidence for major environmental perturbation prior to and during the Toarcian (Early Jurassic) oceanic anoxic event from the Lusitanian Basin, Portugal. Paleoceanography 23, PA1202

Suan, G., van de Schootbrugge, B., Adatte, T., Fiebig, J., Oschmann, W., 2015. Calibrating the magnitude of the Toarcian carbon cycle perturbation. Paleoceanography 30, 495–509.

Swart, P.K., 2015. The geochemistry of carbonate diagenesis: The past, present and future. Sedimentology 62, 1233–1304.

Taylor, H.P., Forester, R.W., 1971. Low-^{18}O igneous rocks from the intrusive complexes of Skye, Mull and Ardnamurchan, Western Scotland. Journal of Petrology 12, 465–497.

Trueman, A.E., 1920. The Liassic rocks of the Cardiff District. Proc. Geol. Assoc. 31, 93–107.

Trueman, A.E., 1922. The Liassic rocks of Glamorgan. Proc. Geol. Assoc. 33, 245–284.

Trueman, A.E., 1930. The lower Lias (Bucklandi Zone) of Nash Point, Glamorgan. Proc. Geol. Assoc. 41, 148–159.

Tyler, J.J., Jones, M., Arrowsmith, C., Allott, T., Leng, M.J., 2016. Spatial patterns in the oxygen isotope composition of daily rainfall in the British Isles. Clim. Dyn. 47, 1971–1987.

Ullmann, C.V., Korte, C., 2015. Diagenetic alteration in low-Mg calcite from macrofossils: a review. Geological Quarterly 59, 3–20.

Ullmann, C.V., Campbell, H.J., Frei, R., Hesselbo, S.P., Pogge von Strandmann, P.A.E., Korte, C., 2013a. Partial diagenetic overprint of Late Jurassic belemnites from New Zealand: Implications for the preservation potential of δ^7Li values in calcite fossils. Geochimica et Cosmochimica Acta 120, 80–96.

Ullmann, C.V., Böhm, F., Rickaby, R.E.M., Wiechert, U., Korte, C., 2013b. The Giant Pacific Oyster (*Crassostrea gigas*) as a modern analog for fossil ostreoids: Isotopic (Ca, O, C) and elemental (Mg/Ca, Sr/Ca, Mn/Ca) proxies. Geochemistry, Geophysics, Geosystems 14 (10), 4109–4120.

Ullmann, C.V., Hesselbo, S.P., Korte, C., 2013c. Tectonic forcing of Early to Middle Jurassic seawater Sr/Ca. Geology 41, 1211–1214.

Ullmann, C.V., Boyle, B., Duarte, L.V., Hesselbo, S.P., Kasemann, S., Klein, T., Lenton, T., Piazza, V., Aberhan, M., 2020 in revision. Warm afterglow from the Toarcian Oceanic Anoxic Event drives the success of deep-adapted brachiopods. Scientific Reports.

van de Schootbrugge, B., Bailey, T.R., Rosenthal, Y., Katz, M.E., Wright, J.D., Miller, K.G., Feist-Burkhardt, S., Falkowski, P., 2005. Early Jurassic climate change and the radiation of organic-walled phytoplankton in the Tethys Ocean. Paleobiology 31, 73–97.

van de Schootbrugge, B. Tremolada, F., Rosenthal, Y., Bailey, T.R., Feist-Burkhardt, S., Brinkhuis, H., Pross, J., Kent, D.V., Falkowski, P.G., 2007. End-Triassic calcification crisis and blooms of organic-walled 'disaster species'. Palaeogeography, Palaeoclimatology, Palaeoecology 244, 126–141.

van de Schootbrugge, B., Payne, J.L., Tomasovych, A., Pross, J., Fiebig, J., Benbrahim, M., Föllmi, K.B., Quan, T. M., 2008. Carbon cycle perturbation and stabilization in the wake of the Triassic-Jurassic boundary mass-extinction event. Geochem. Geophys. Geosyst., 9, Q04028.

van de Schootbrugge, B., Quan, T.M., Lindström, S., Püttmann, W., Heunisch, C., Pross, J., Fiebig, J., Petschick, R., Röhling, H.-G., Richoz, S., Rosenthal, Y., Falkowski, P.G.,

2009. Floral changes across the Triassic/Jurassic boundary linked to flood basalt volcanism. Nature Geoscience 2, 589–594.

van de Schootbrugge, B., Bachan, A., Suan, G. Richoz, S. Payne, J.L., 2013. Microbes, mud and methane: cause and consequence of recurrent Early Jurassic anoxia following the end-Triassic mass extinction. Palaeontology 56, 685–709.

van de Schootbrugge, B., Richoz, S., Pross, J., Luppold, F.W., Hunze, S., Wonik, T., Blau, J., Meister, C., Van der Weijst, C.M.H., Suan, G., Fraguas, A., Fiebig, J., Herrle, J.O., Guex, J., Little, C.T.S., Wignall, P.B., Püttmann, W., Oschmann, W., 2019. The schandelah scientific drilling project: A 25-million year record of early Jurassic palaeoenvironmental change from northern Germany. Newsletters on Stratigraphy 52, 249–296.

Warrington, G., Ivimey-Cook, H.C., 1995. The Late Triassic and Early Jurassic of coastal sections in west Somerset and South and Mid-Glamorgan. In: Taylor, P.D. (Ed.) Field Geology of the British Jurassic, pp. 9–30. London: The Geological Society.

Weedon, G.P., Jenkyns, H.C., Page, K.N., 2018. Combined sea-level and climate controls on limestone formation, hiatuses and ammonite preservation in the Blue Lias Formation, South Britain (uppermost Triassic – Lower Jurassic). Geological Magazine 155, 1117–49.

Weedon, G.P., Page, K.N., Jenkyns, H.C., 2019. Cyclostratigraphy, stratigraphic gaps and the duration of the Hettangian Stage (Jurassic): Insights from the Blue Lias Formation of southern Britain. Geological Magazine 156, 1469–1509.

Whittaker, A., Green, G.W., 1983. Geology of the Country around Weston-super-Mare. Memoir for the 1:50000 Geological Sheet 279, new series with parts of sheets 263 and 295. London: HMSO.

Wignall, P.B., Hallam, A., 1991. Biofacies, stratigraphic distribution and depositional models of British onshore Jurassic black shales. In: Tyson, R.V., Pearson, T. H. (Eds.), Modern and Ancient Continental Shelf Anoxia, Special Publication of the Geological Society of London 58, 291–309.

Wilson D., Davies, J.R., Fletcher, C.J.N., Smith, M., 1990. Geology of the South Wales Coalfield, Part VI, the country around Bridgend. Memoir of the British Geological Survey, 1:50 000 Geological Sheets 261 and 262 (England and Wales), pp. 1-62, British Geological Survey, Aberystwyth.

Wotzlaw, J.-F., Guex, J., Bartolini, A., Gallet, Y., Krystyn, L., McRoberts, C.A., Taylor, D., Schoene, B., Schaltegger, U., 2014. Towards accurate numerical calibration of the

Late Triassic: High-precision U-Pb geochronology constraints on the duration of the Rhaetian. Geology 42 (7), 571–574.

Xu, W., Ruhl, M., Hesselbo, S.P., Riding, J.B., Jenkyns, H.C., 2016. Orbital pacing of the Early Jurassic carbon cycle, black-shale formation and seabed methane seepage, Sedimentology 64, 127–149.

Yager, J.A., West, A.J., Corsetti, F.A., Berelson, W.M., Rollins, N.E., Rosas S., Bottjer, D.J., 2017. Duration of and decoupling between carbon isotope excursions during the end-Triassic mass extinction and Central Atlantic Magmatic Province emplacement. Earth and Planetary Science Letters 473, 227–236.

Ziegler, P.A., 1990. Geological Atlas of Western and Central Europe (second edition). The Geological Society for Shell Internationale Petroleum Maatschppij B.V., The Hague.

Figure captions

Fig. 1. (A) Early Jurassic palaeogeographical setting (modified after Damborenea (2002) and Dera et al., (2009); the study area shown by a red star lies within the N-S oriented Laurasian Seaway that connected the equatorial Tethys Ocean to the north polar Boreal Sea via a Viking Corridor. (B) Timescale for the Hettangian–Sinemurian stages (Gradstein et al., 2012; Wotzlaw et al., 2014) and lithostratigraphy for study sites in the Bristol Channel Basin (Cox et al., 1999) and Hebrides Basin (Hesselbo et al., 1998). Grey shading indicates approximate age uncertainty (Gradstein et al., 2012). (C) Location map for Lochaline (Morvern), Boreraig and Ardnish (Isle of Skye), and Hallaig Waterfall (Isle of Raasay); all localities represent deposition in the Hebrides Basin. Dark grey fields represent central igneous complexes. (D) Location map for St Audrie's Bay to East Quantoxhead (Somerset), and Nash Point (Glamorgan). Lyme Regis and Lavernock localities, referred to in text, are also shown. All localities represent deposition in the Bristol Channel Basin, except Lyme Regis which is in the Wessex Basin. See text for precise locality information.

Fig. 2. Summary lithology, biostratigraphy and carbon isotope data from calcite fossils from the present study for the Somerset succession, including the Hettangian at St Audrie's Bay and the Hettangian and lower Sinemurian at East Quantoxhead. Biostratigraphy from Bloos and Page (2002) and Weedon et al. (2019). Lithological succession from Whittaker and Green (1983), Hesselbo et al. (2004), Xu et al. (2016), Weedon et al.

(2018), and authors' own unpublished observations). For lithological key see Fig. 3. Tr. = Triassic. Rh. = Rhaetian. See text for precise locality information.

Fig. 3. Summary lithology, biostratigraphy and carbon isotope data from calcite fossils from the present study for Lochaline (Morvern), Boreraig and Ardnish (Isle of Skye), and Hallaig Waterfall (Isle of Raasay). AI = Ardnish Ironstone. All stratigraphy based on Hesselbo et al. (1998).

Fig. 4. SEM images from a selection of analysed calcite fossils. (A–D) Well preserved oyster shells (A: sample Alt-L 42; B: sample KV 10 A; C: Hal 61; D: Ard 121). (E, F) Strongly altered bivalves from Boreraig (E: oyster shell, Bor 137; F: pinnid shell, Bor 101). All scales 100 μm.

Fig. 5. Compilation of macrofossil $\delta^{13}C$ and $\delta^{18}O$ values for all calcite fossils for the complete Hettangian and lower Sinemurian interval from the UK (including data from Korte et al., 2009). Samples originate from St Audrie's Bay, East Quantoxhead and Watchet (all Somerset), Lavernock Point and Nash Point (Wales), Lochaline (Movern, Scotland), Ardnish and Boreraig (Isle of Skye, Scotland), and Hallaig Waterfall (Raasay, Scotland). Two astronomical age models are available for the Hettangian (Ruhl et al., 2010; Weedon et al., 2019), but these differ significantly from each other; there is not yet an astronomical age model for the Sinemurian. For simplicity and correspondence to previously published data from this interval, all data are plotted against the ammonite subzone number as tabulated in the associated data files. Bulk rock carbon-isotope data are shown from the Llanbedr (Mochras Farm) borehole, N Wales (Storm et al., 2020). All data are plotted assuming constant sedimentation rates between zone or subzone boundaries. *tilm.* = *tilmanni*.

Fig. 6 Box and whisker plots for data shown in Figure 5, excluding only oxygen isotope data from the Skye localities of Ardnish and Boreraig, where a proportion of the analysed shells are probably affected by hydrothermal alteration. Boxes are second and third quartile; whiskers are 2.5-97.5 % range, thick black line is median. Numbers at end of whiskers are number of analyses and are gathered by ammonite subzone. Colour coding of oxygen boxes is according to median value. Note the divergent trend between carbon and oxygen isotope values from the late Hettangian onwards, predominantly defined by progressively heavier carbon-isotope values, especially across the Hettangian–Sinemurian boundary. This data treatment necessarily masks evident fluctuations at higher frequencies. An indicative scale of relative temperature change is added for oxygen-isotope data using the Anderson and Arthur (1983)

equation and assumed -1 permil for $\delta^{18}O_{seawater}$; the normal caveat for oxygen-isotope data from marine macrofossil calcite applies, in that factors other than temperature may be significant. However, as argued in the text, we interpret temperature change to be the predominant factor in this case. *til*. = *tilmanni*, *plan*. = *planorbis*, *lias*. = *liasicus*, *semicost*. = *semicostatum*.

Fig. 7 Co-variation of carbon and oxygen isotope ratios with Mn/Ca ratios in shell calcite from Hallaig Waterfall (dark blue), Ardnish (pale blue), and Boreraig (white) from the *lyra* Subzone of the *semicostatum* Zone. Alteration of isotopic ratios is poorly described by Mn/Ca ratios and is only apparent in $\delta^{18}O$ values. (A) Carbon isotope ratios show little covariance with Mn/Ca ratios and are consistent at all three locations. (B) Oxygen isotope ratios of the three locations plot in distinct fields. Intermediate ^{18}O depletion of shell calcite from Ardnish and strong depletion from Boreraig are notable.

Associated Dataset (Deposited in Mendeley Data)

Table 1: Stratigraphic positions and relative positions in related subzones, material analysed, carbon- and oxygen-isotope values, and element ratios of analysed samples. Isotope values were analyzed in Copenhagen (C), Innsbruck (Inn), Oxford (Ox), and Bochum (Bo).

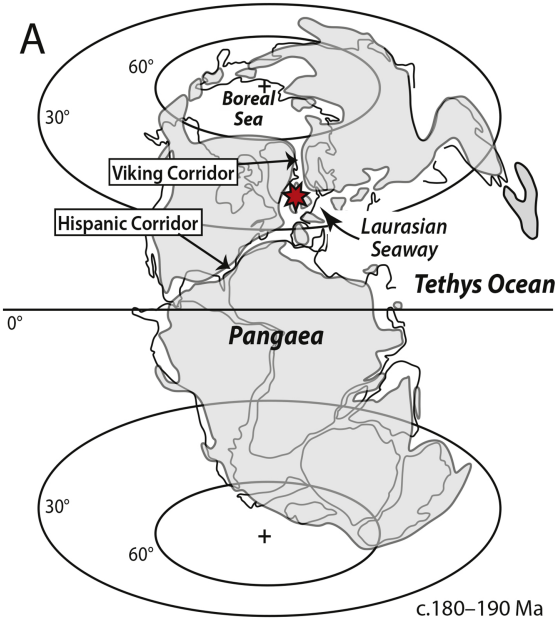
A
60°
30°
Boreal Sea
Viking Corridor
Hispanic Corridor
Laurasian Seaway
Tethys Ocean
0°
Pangaea
30°
60°
c.180–190 Ma

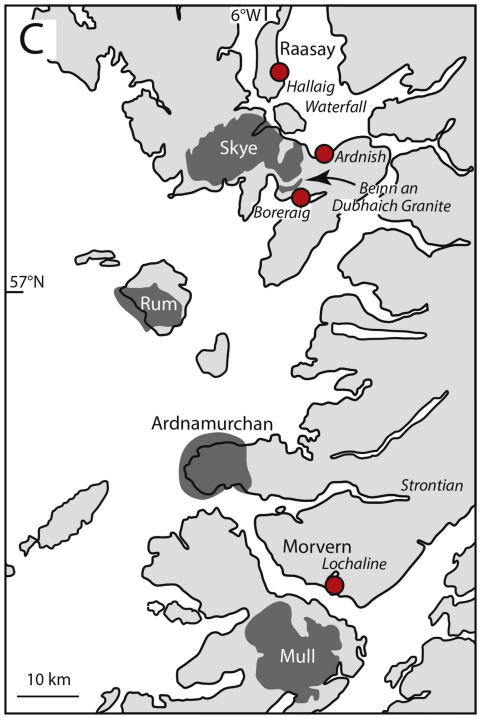
C
6°W
Raasay
Hallaig
Waterfall
Skye
Ardnish
Beinn an
Dubhaich Granite
Boreraig
57°N
Rum
Ardnamurchan
Strontian
Morvern
Lochaline
Mull
10 km

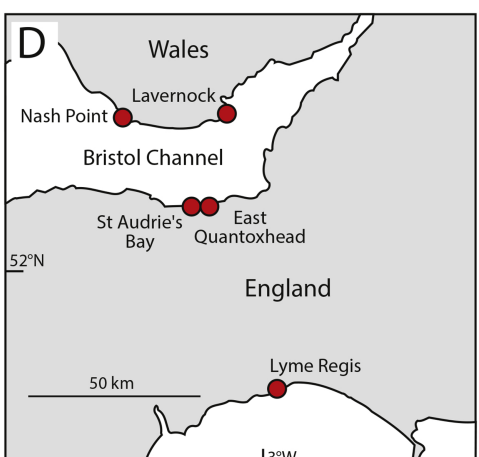
D
Wales
Lavernock
Nash Point
Bristol Channel
St Audrie's
Bay
East
Quantoxhead
52°N
England
50 km
Lyme Regis
3°W

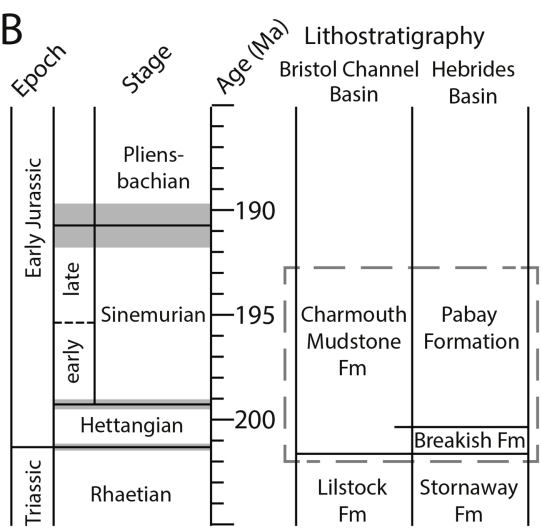
B
Epoch
Stage
Age (Ma)
Lithostratigraphy
Bristol Channel Basin
Hebrides Basin
Early Jurassic
Triassic
late
early
Pliens-
bachian
Sinemurian
Hettangian
Rhaetian
190
195
200
Charmouth
Mudstone
Fm
Pabay
Formation
Breakish Fm
Lilstock
Fm
Stornaway
Fm

Figure 1

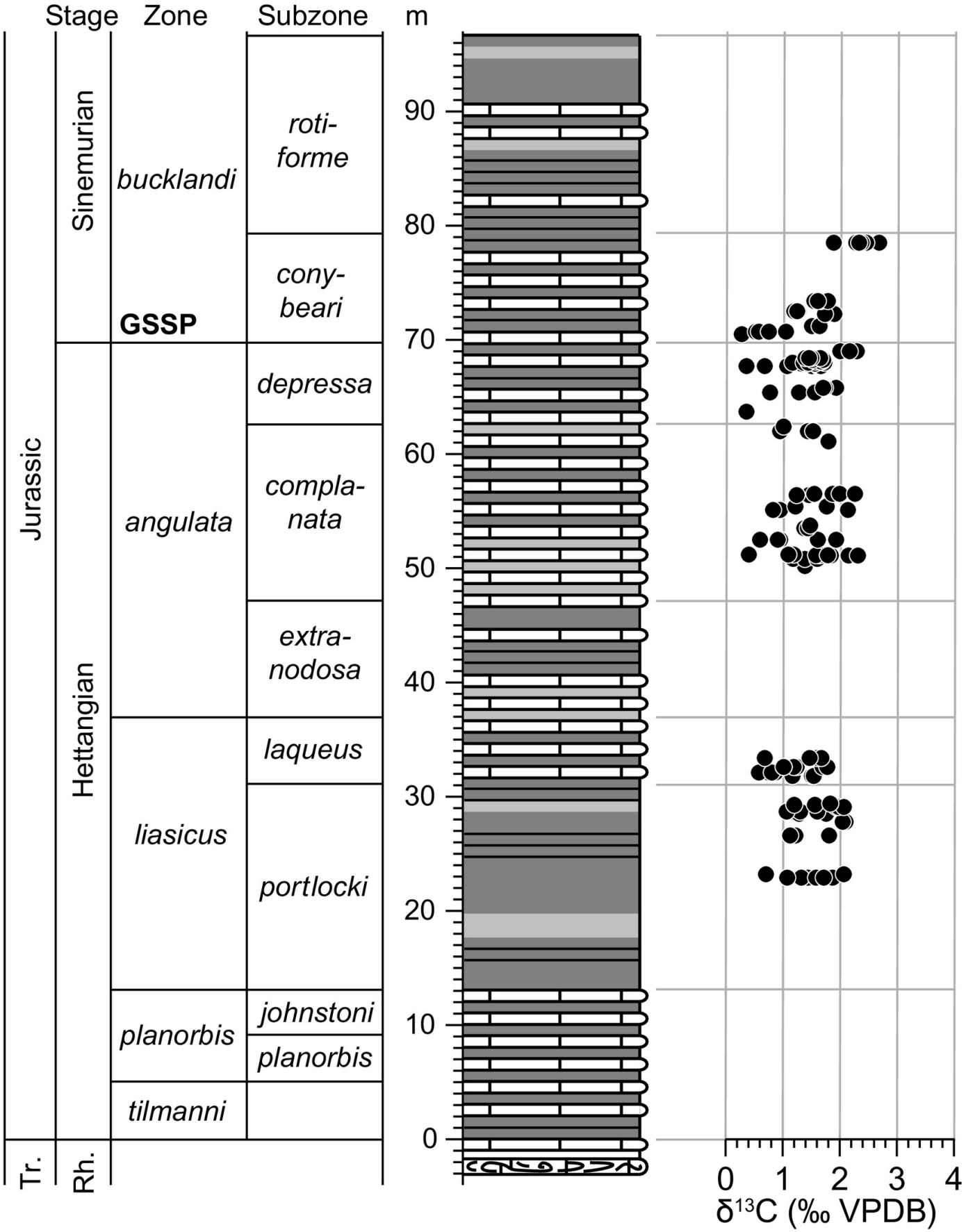
Stage
Zone
Subzone
m
Jurassic
Sinemurian
Hettangian
Tr.
Rh.
bucklandi
GSSP
angulata
liasicus
planorbis
tilmanni
roti-forme
cony-beari
depressa
compla-nata
extra-nodosa
laqueus
portlocki
johnstoni
planorbis
90
80
70
60
50
40
30
20
10
0
0 1 2 3 4
δ13C (‰ VPDB)

Figure 2

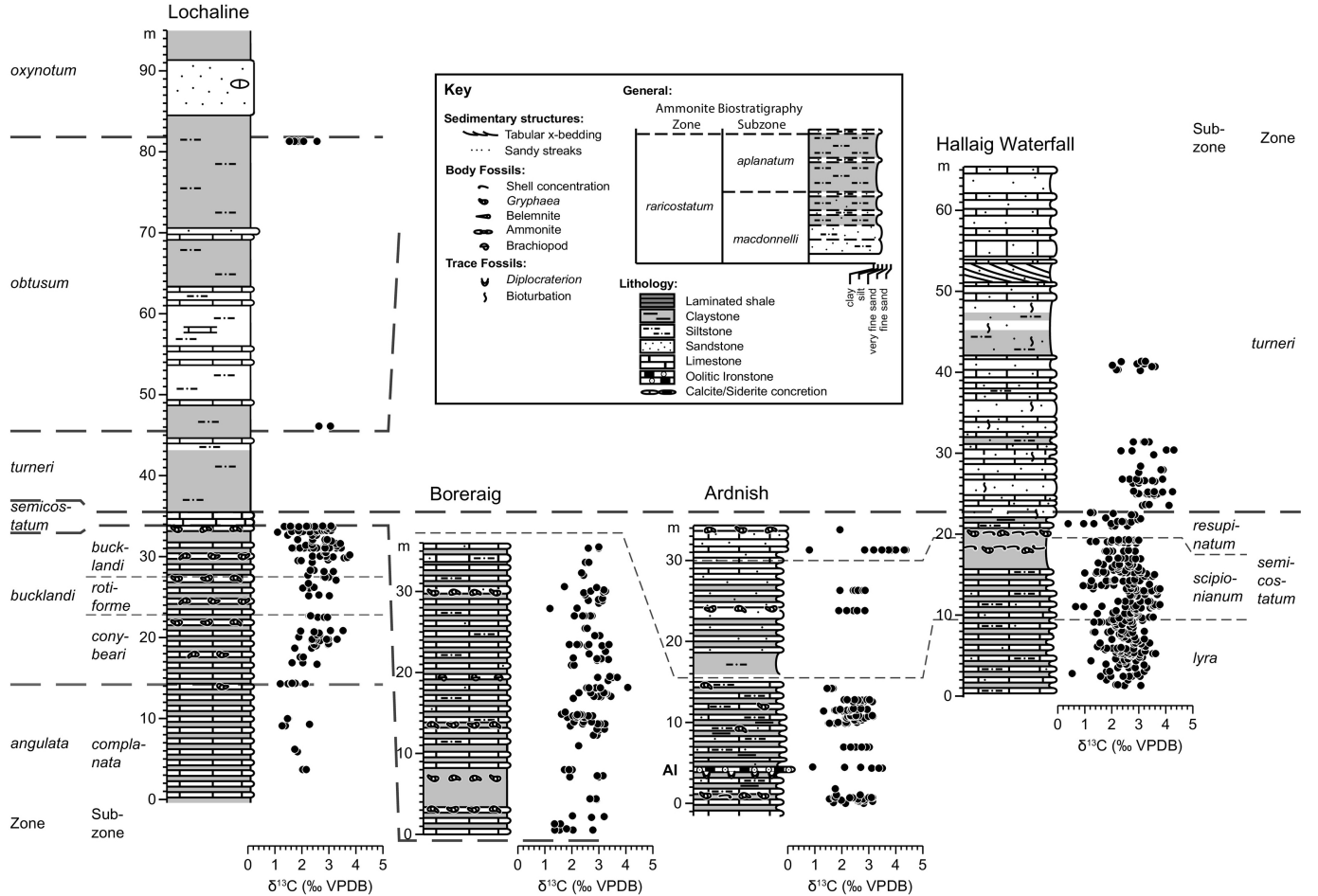
Lochaline
Boreraig
Ardnish
Hallaig Waterfall
Key
Sedimentary structures:
Tabular x-bedding
Sandy streaks
Body Fossils:
Shell concentration
Gryphaea
Belemnite
Ammonite
Brachiopod
Trace Fossils:
Diplocraterion
Bioturbation
General:
Ammonite Biostratigraphy
Zone
Subzone
raricostatum
aplanatum
macdonnelli
Lithology:
Laminated shale
Claystone
Siltstone
Sandstone
Limestone
Oolitic Ironstone
Calcite/Siderite concretion
clay
silt
very fine sand
fine sand
oxynotum
obtusum
turneri
semicos-tatum
buck-landi
bucklandi
roti-forme
cony-beari
angulata
compla-nata
Zone
Sub-zone
resupi-natum
scipio-nianum
lyra
semi-cos-tatum
Al
m
δ13C (‰ VPDB)

Figure 3

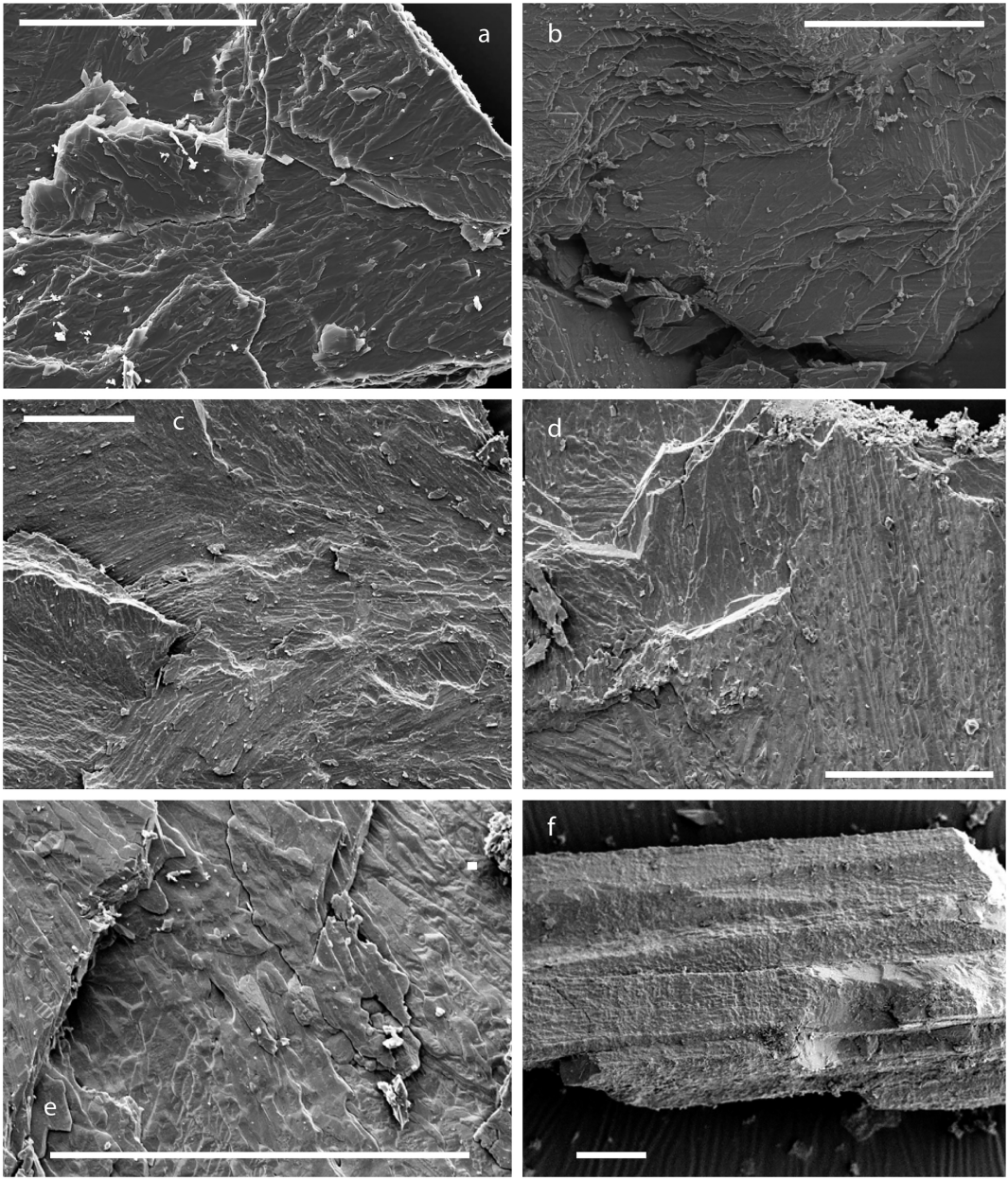

Figure 4

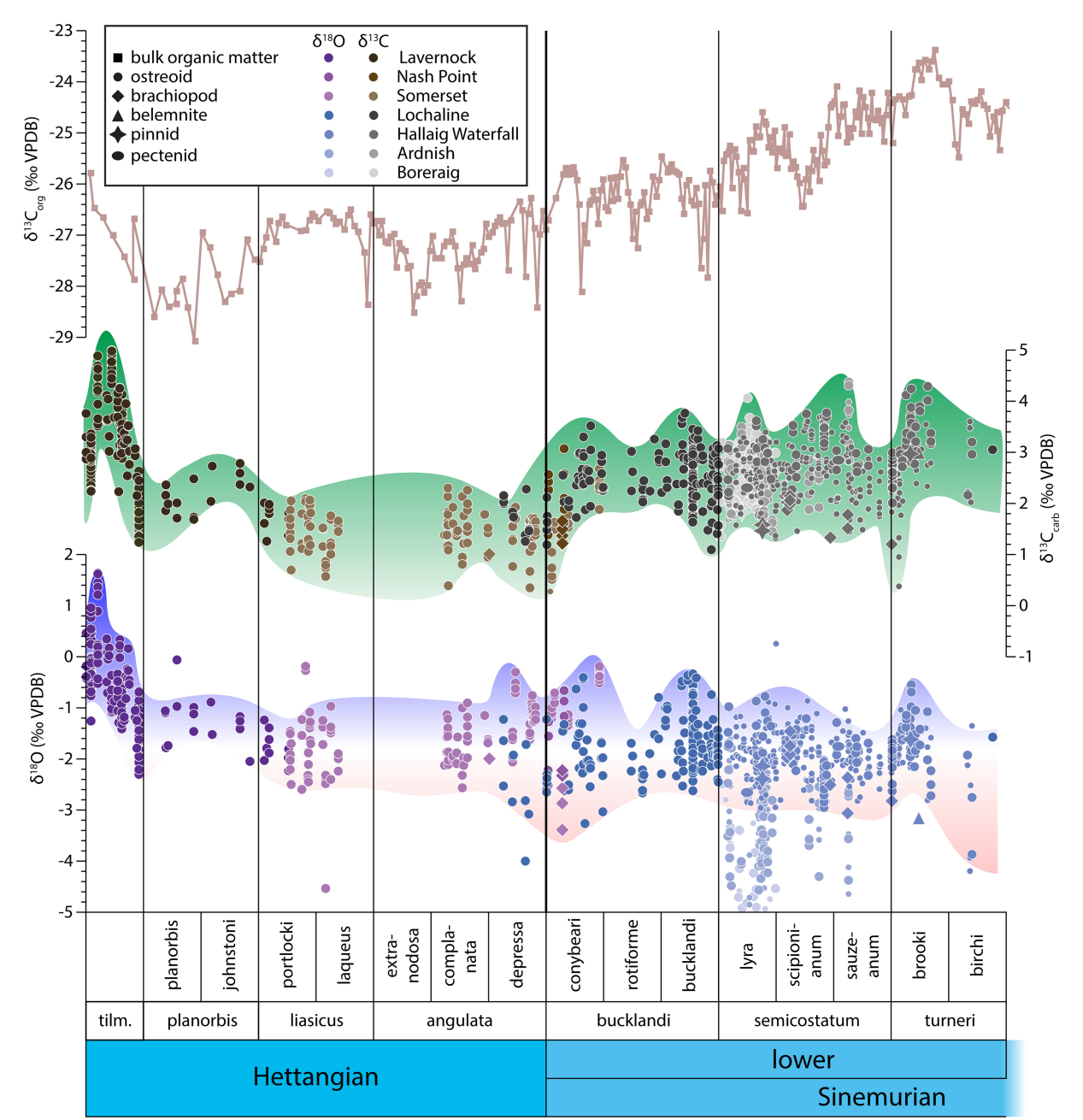
bulk organic matter
ostreoid
brachiopod
belemnite
pinnid
pectenid
δ18O δ13C
Lavernock
Nash Point
Somerset
Lochaline
Hallaig Waterfall
Ardnish
Boreraig
δ13Corg (‰ VPDB)
δ13Ccarb (‰ VPDB)
δ18O (‰ VPDB)
tilm.
planorbis
johnstoni
portlocki
laqueus
extra-nodosa
compla-nata
depressa
conybeari
rotiforme
bucklandi
lyra
scipioni-anum
sauze-anum
brooki
birchi
tilm.
planorbis
liasicus
angulata
bucklandi
semicostatum
turneri
Hettangian
lower
Sinemurian

Figure 5

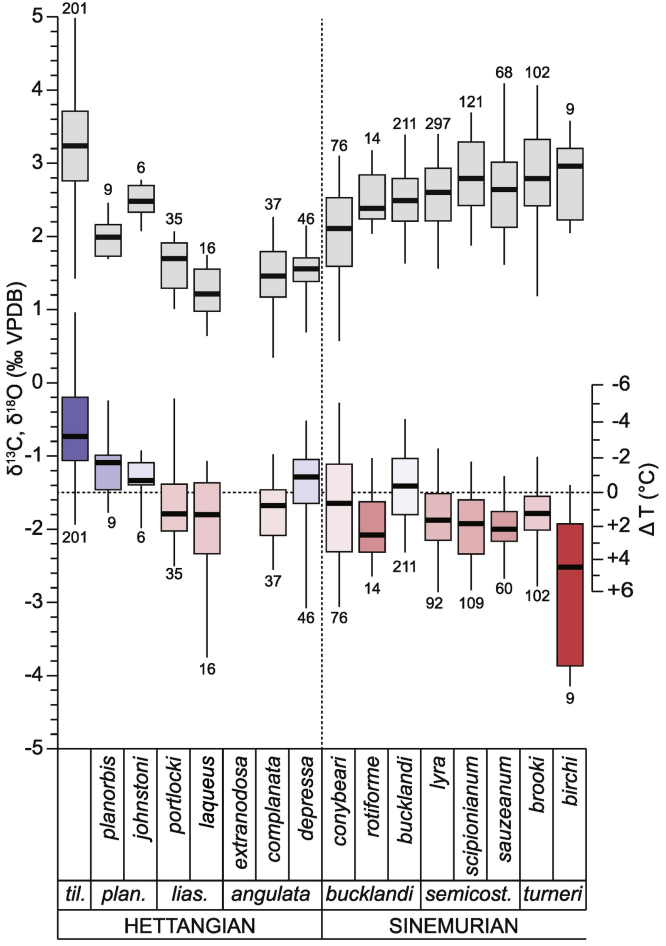
δ13C, δ18O (‰ VPDB)
ΔT (°C)
5
4
3
2
1
0
-1
-2
-3
-4
-5
-6
-4
-2
0
+2
+4
+6
201
9
6
35
16
37
46
76
14
211
297
121
68
102
9
92
109
60
til.
plan.
lias.
angulata
bucklandi
semicost.
turneri
planorbis
johnstoni
portlocki
laqueus
extranodosa
complanata
depressa
conybeari
rotiforme
bucklandi
lyra
scipionianum
sauzeanum
brooki
birchi
HETTANGIAN
SINEMURIAN

Figure 6

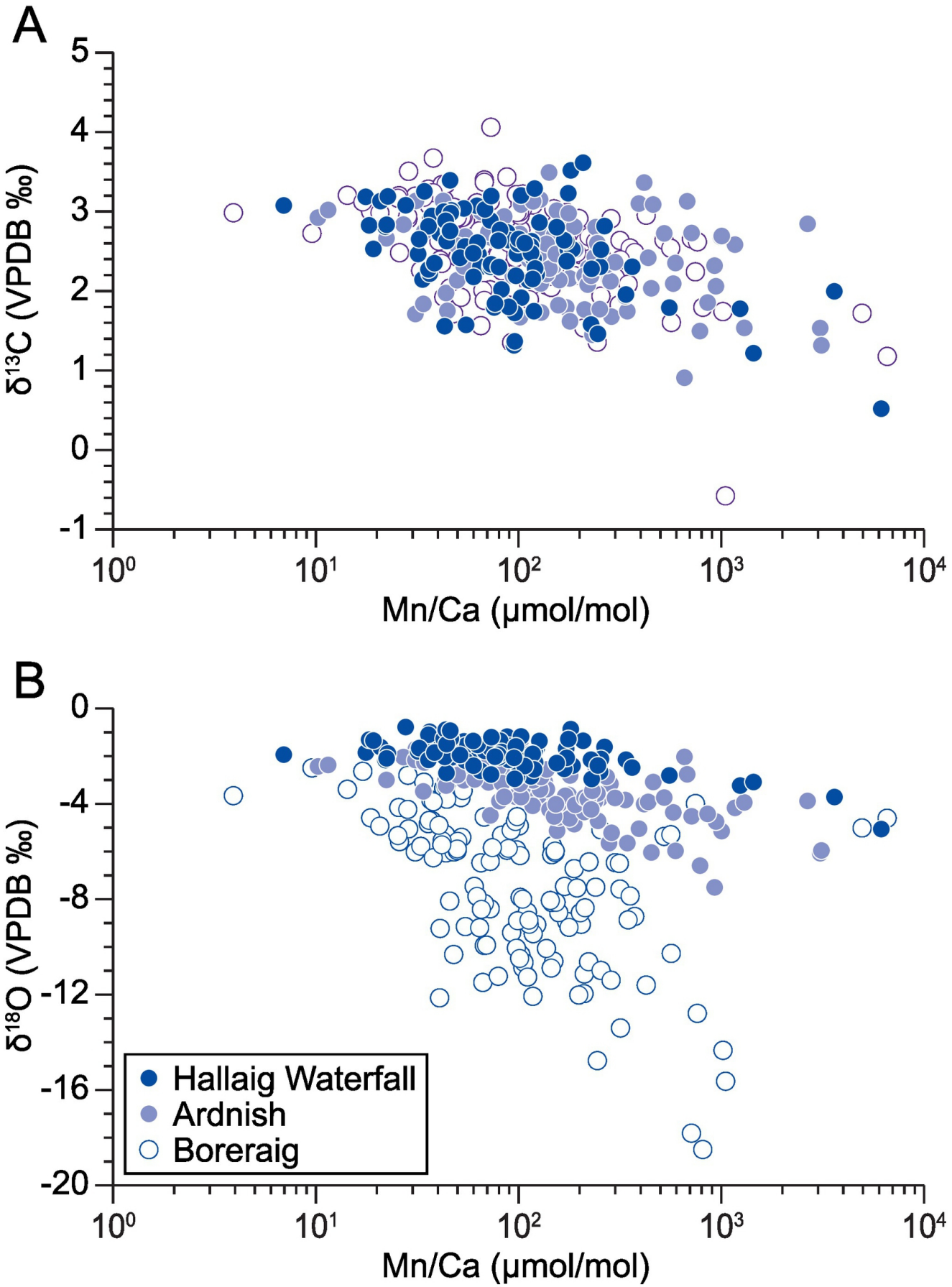
A
5
4
3
2
1
0
-1
δ13C (VPDB ‰)
10^0
10^1
10^2
10^3
10^4
Mn/Ca (µmol/mol)
B
0
-4
-8
-12
-16
-20
δ18O (VPDB ‰)
Hallaig Waterfall
Ardnish
Boreraig
10^0
10^1
10^2
10^3
10^4
Mn/Ca (µmol/mol)

Figure 7